Analyzing power measurement for the $^{14}N(\vec{p}, \gamma)^{15}O$ reaction at astrophysically relevant energies

S. O. Nelson,[1,2] M. W. Ahmed,[1,2] B. A. Perdue,[1,2] K. Sabourov,[1,2] A. L. Sabourov,[1,2] A. P. Tonchev,[1,2] R. M. Prior,[3,2] M. Spraker,[3,2] and H. R. Weller[1,2]

[1]*Department of Physics, Duke University, Durham, North Carolina 27708, USA*

[2]*Triangle Universities Nuclear Laboratory, Duke Station, Durham, North Carolina 27708, USA*

[3]*Department of Physics, North Georgia College and State University, Dahlonega, Georgia 30597, USA*

(Received 18 August 2003; published 18 December 2003)

The $^{14}N(\vec{p}, \gamma)^{15}O$ reaction has been investigated by measuring the angular distributions of its cross section and analyzing power using a 270-keV polarized proton beam. Calculations using a direct-capture-plus-resonance model were compared with the data. The results indicate the presence of γ transition amplitudes which were not considered in previous extrapolations of the astrophysical S factor to low energies. The impact on the zero-energy S factor of the $^{14}N(\vec{p}, \gamma)^{15}O$ reaction is discussed.

DOI: 10.1103/PhysRevC.68.065804 PACS number(s): 26.20.+f

I. INTRODUCTION

The reaction $^{14}N(p, \gamma)^{15}O$ is the slowest reaction in the hydrogen burning carbon-nitrogen-oxygen (CNO) cycle, making it the reaction that governs the cycle's total rate of energy production [1]. In a stellar plasma, most of the hydrogen burning for this reaction takes place in an energy range where the decrease of the number of colliding particles at higher energies competes with the decrease in the probability that an incident particle will tunnel through the coulomb barrier at lower energies. This energy range, the Gamow window, depends on the temperature of the plasma and the masses and charges of the nuclei in a particular reaction. The total reaction rate in a stellar plasma depends on the structure of the reaction cross section within the window. For stars where the $^{14}N(p, \gamma)^{15}O$ reaction controls energy production, the Gamow window falls somewhere in the range of $E_{\text{c.m.}} = 30-100$ keV.

Previous measurements of the reaction cross section have been performed at 200 keV and above [2]. The sole exception is an activation measurement using 100–135 keV protons [3], the results of which are close to a factor of 2 larger than recent extrapolations of the total cross section to these energies [2,4], and which provides no information about the modes of capture. The $^{14}N(p, \gamma)^{15}O$ reaction has been observed to be dominated by capture to the 6.793-MeV excited state of ^{15}O [2] below 200 keV. This strength has been interpreted as arising from a direct-capture component, along with a contribution from the tail of the $E_{\text{c.m.}} = 259$-keV resonance [4]. This resonance corresponds to the 7.556-MeV ($J^{\pi} = 1/2^{+}$) state in ^{15}O, as shown in Fig. 1.

The availability of intense beams of polarized protons at TUNL has made it possible to measure the analyzing power A_y [5] for the $^{14}N(\vec{p}, \gamma)^{15}O$ reaction, defined as

$$A_y = \frac{Y_+ - Y_-}{p_- Y_+ + p_+ Y_-}, \tag{1}$$

where Y_+ and Y_- are the yields of γ rays from the $^{14}N(\vec{p}, \gamma)^{15}O$ reaction with the protons polarized in the positive and negative $\hat{y}$ directions, and p_+ and p_- are the magnitudes of those polarizations. The $\hat{y}$ axis is defined according to the Madison convention [6] by $\hat{k}_{in} \times \hat{k}_{out}$, where $\hat{k}_{in}$ is in the direction of the proton beam and $\hat{k}_{out}$ is in the direction of the γ ray. The angular distribution of the analyzing power is sensitive to interference between the contributing amplitudes, and can provide information about the amplitudes of the γ-decay multipoles which contribute to the capture process.

It should also be noted that the analyzing power is relatively insensitive to systematic errors. Errors in detector efficiency and effective solid angle which plague cross section measurements cancel out in the analyzing power, leaving four principal sources of error. The first is the statistical error. The error in the counts from the subtracted spectrum in the region of interest is determined from propagation of the errors in the gross counts in the two raw spectra (data and background) within the region of interest. Such a statistical error is the dominant source of error in the present work. A second source of error arises in the case where there is significant interference from the Compton edges of nearby capture peaks. In the present case, the peaks of significant strength are well separated in energy and the peak-to-

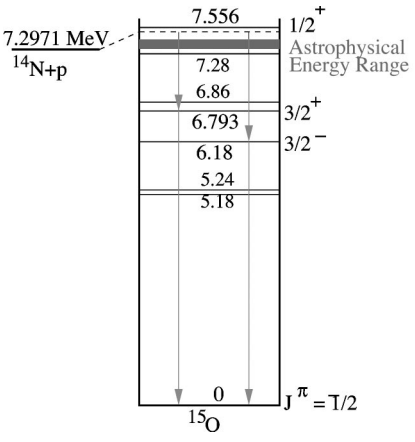

Level	S(0) (keV b)
7.28	0.022
6.86	0.042
6.79	1.63
6.18	0.06
5.24	0.018
5.18	0.014
0.00	0.08

FIG. 1. The structure of ^{15}O, showing the energy range of most astrophysical interest, the two modes of capture investigated in the present work, and the astrophysical S factors [$S(0)$] for capture to bound states of ^{15}O for the $^{14}N(p, \gamma)^{15}O$ reaction [2,4].

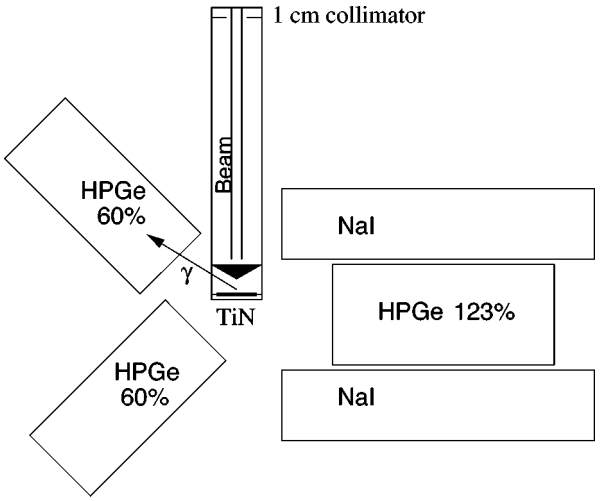

FIG. 2. The experimental setup.

Compton ratio for our large high purity germaniums (HPGe's) is sufficiently high so that this error is negligibly small. We calculate that it has less than a 1% effect, based on the standard detector response function for these detectors. The most significant systematic error in an analyzing power measurement remains the error in the measurement of the polarization of the protons. Our polarization is monitored via the spin-filter polarimeter [7] on the TUNL Atomic Beam Polarized Ion Source (ABPIS) [8]. From a comparison of calibrated polarimeters, Ref. [7] finds an accuracy in the polarization of better than 3%, which we adopt in the present work. The last and least significant error arises from having a different number of protons incident on the target for each spin state. A charge integrator and scaler were used to measure the total deposited charge for each spin state and normalize the yield (only a 0.4% change) to a negligibly small error.

The analyzing power at θ=90° is nonzero only in the presence of interference between decay modes of opposite parity (e.g., $E1$ with $M1$ or $E2$). In this work we will present the first polarized proton beam studies of the ^{14}N$(\vec{p},\gamma)^{15}$O reaction below 270 keV. We will examine transitions to the 6.793- and 6.176-MeV states in ^{15}O, which are displayed in Fig. 1. The results will be used to investigate which amplitudes are actually present in the reaction, and to test previous models of the reaction.

II. EXPERIMENTAL SETUP

A beam of 80-keV polarized H^- ions was obtained from the TUNL ABPIS [8]. The polarization was measured using the spin-filter polarimeter and found to be $|p_y|=0.8\pm0.03$ [7], and the direction of polarization was reversed at 1 Hz. After passing through an analyzing magnet, the ions were accelerated to 270 keV (lab frame) in the TUNL minitandem. The collimated proton beam was subsequently stopped in a thick target of compressed TiN powder, as shown in Fig. 2. γ rays from the ^{14}N$(\vec{p},\gamma)^{15}$O reaction were detected by HPGe detectors at 45°, 90°, and 135°.

The detectors at 45° and 135° were 60% efficient relative to a 3 in.$\times$3 in. NaI detector, and the one at 90° was 123% efficient. The detector distances were chosen to keep the finite geometry coefficient Q_2 above 0.9 [9]. Background in all detectors was reduced by 10 cm of passive lead shielding. The 90° detector was also outfitted with a NaI annulus to reduce cosmic ray, room background, and Compton scattered events. The target was replaced with a ^{228}Ra source in order to measure the relative efficiencies of the three HPGe's. The relative intensities of γ-ray lines from this source are known [10], and the relative number of counts in the γ-ray lines observed in each detector made it possible to determine the relative efficiencies for all three detectors at the median energies of the two γ-ray peaks of interest. This measurement of relative efficiencies was used to correct the angular distribution of the cross section for detector efficiency and γ-ray attenuation in the present geometry.

III. DATA AND DIRECT CAPTURE PLUS RESONANCE MODEL CALCULATIONS

Stopping the beam in the target produces a spread of proton energies from 252 to 0 keV (center-of-mass frame), corresponding to a spread in γ-ray energies for capture to each final state. The γ energies are related to the energies of the captured protons by $E_\gamma=Q+E_{\rm c.m.}$ For capture to the 6.793-MeV state, 0.504 MeV$<E_\gamma<$0.756 MeV. For capture to the 6.176-MeV state, 1.211 MeV$<E_\gamma<$1.373 MeV. The differential yield $dy(E)$ of γ rays from proton capture reactions, for a proton beam of energy E which loses energy dE in a thick target, is given by

$$dy(E)=\frac{\sigma(E)}{\mathrm{stp}(E)}N_p dE, \tag{2}$$

where N_p is the number of protons incident on the target, stp(E) is the proton stopping power of TiN [11], and $\sigma(E)$ is the energy-dependent cross section. Using the astrophysical S factors $[S(E)]$ of Ref. [4] and the relation

$$\sigma(E_{\rm c.m.})=S(E_{\rm c.m.})e^{-2\pi\eta}/E_{\rm c.m.}, \tag{3}$$

where η is the Sommerfeld parameter $[2\pi\eta=212.4/\sqrt{E_{\rm c.m.}}$ for the ^{14}N$(p,\gamma)^{15}$O reaction with $E_{\rm c.m.}$ in keV], we integrate Eq. (2) and find that over 90% of the emitted γ rays are generated by protons in the top 40 keV for protons with $E_{\rm c.m.}=252$ keV. This 40 keV energy spread, with small ($\approx$2 keV) additions to account for the detectors' energy resolutions (as observed in the room background lines), provides limits for our range of summation for the yields. Detected γ rays were sorted into spin-up and spin-down spectra. The background spectra, taken with the beam off, were normalized to time and subtracted from the beam-on spectra. The thick-target analyzing powers were determined using the yields (sums from the top $\approx$40 keV of each spectrum) and measured beam polarization as inputs to Eq. (1).

We will also define an effective energy E_{eff} for the present measurement as the proton energy in the center-of-mass frame corresponding to the median energy of the γ peak, where half the counts are due to protons above this energy.

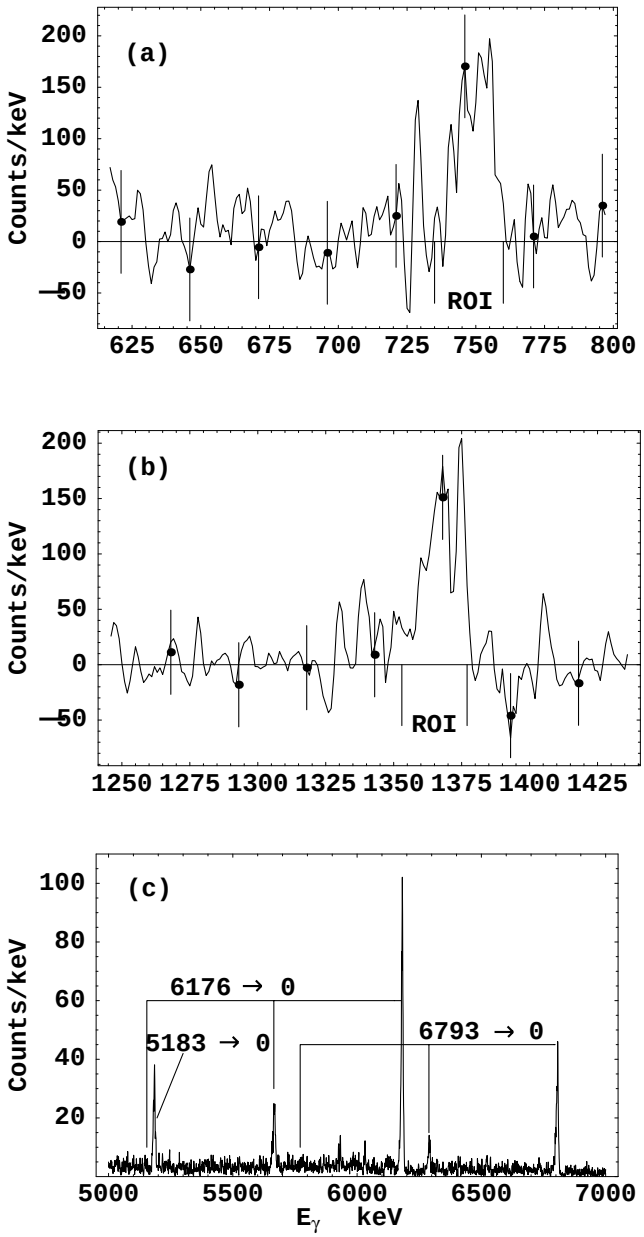

FIG. 3. Spectra for capture to the 6.793 (a) and 6.176 MeV (b) states and the decay of the bound states to the ground state (c). Sample error bars are shown every 25 keV. The region of interest ("ROI") is denoted by the labeled vertical bars in plots (a) and (b). This is the region used for summation in calculating the analyzing power.

Using S factors from Ref. [2] (which we will show are consistent with our calculated S factor above 200 keV), the effective energy for capture to the 6.793-MeV state is 245 keV, while it is 248 keV for capture to the 6.176-MeV state.

Examples of background-subtracted spectra near 750 and 1370 keV can be seen in Fig. 3, and display the capture lines leading to the 6.793- and 6.176-MeV states. The decays of these two excited states to the ground state are also shown in Fig. 3. Although decays from the 5.183-MeV state were also observed, the detector efficiency for the $\approx$2.36-MeV γ rays from capture *to* this state is considerably lower than for capture to the other two prominent states. The resulting (low) counting statistics for capture to this state make those data of little value.

TABLE I. Optical model parameters for generating the scattering-state wave functions.

V_{opt}	W_{opt}	V_{SO}	r_0	a
67	4	6	1.3	0.6

The angular distribution of the cross section and analyzing power were modeled with the direct-capture-plus-resonance (DCPR) code HIKARI. Details of the computational model may be found in Ref. [12]. The direct-capture calculations used an optical model potential to generate distorted waves to describe the incident proton and a Woods-Saxon potential to calculate the radial bound-state wave functions. Resonances are added as Breit-Wigner resonance amplitudes. The optical model potential parameters are given in Table I. The bound-state potential parameters for each final state (labeled by $E_{F.S.}$) are given in Table II. The depth of the bound-state potential (V_0, Table II) is calculated by HIKARI from the binding energy of the final state, other parameters are user-defined inputs. All energies are in MeV and all distances in femtosecond. Both real potentials are described by the Woods-Saxon form:

$$V(r) = -\frac{V_0}{1+e^{(r-R)/a}}, \tag{4}$$

where the magnitude of the potential is given by V_0, the radius $R=r_0A^{1/3}$, and a is the diffuseness. For the optical potential, the imaginary potential is the scaled derivative of the real potential, $W(r)=dV(r)/dr(W_{opt}/V_{opt})$. A spin-orbit potential with strength V_{SO} was also included in the scattering and the bound-state potentials.

For comparison to previously published values [13], we give (below) the proton and γ widths (Γ_p and Γ_γ, respectively) which were used in the present calculations. The strengths, $\omega\gamma$, of the contributing resonances are related to these widths by $\omega\gamma=[2J+1/(2I_1+1)(2I_2+1)](\Gamma_p\Gamma_\gamma/\Gamma)$, where J is the angular momentum of the resonance, I_1 and I_2 are the spins of the proton and target nucleus, and $\Gamma=\Gamma_p+\Gamma_\gamma$ is the total width of the resonance. Angular distributions of cross section and analyzing power are calculated after Ref. [5]. In order to be consistent with the energy spread of the protons in the target, the calculated angular distributions of the cross section and analyzing power shown have been integrated

TABLE II. Woods-Saxon potential parameters for generating the radial bound-state wave functions.

$E_{F.S.}$	V_0	V_{SO}	r_0	r_c	a
6.793	53.8	2	1.3	1.2	0.6
6.176	32.6	2	1.3	1.2	0.6

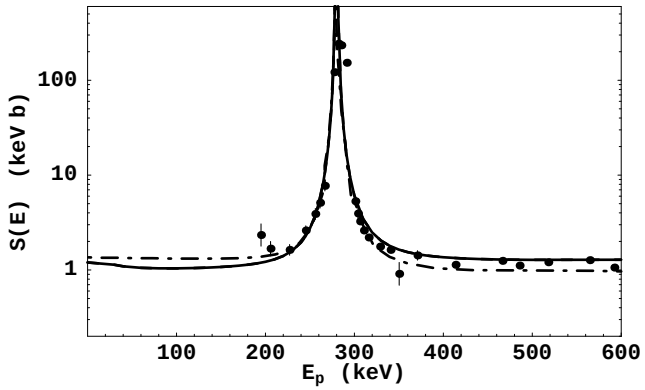

FIG. 4. The astrophysical S factor for capture to the 6.793-MeV state in ^{15}O in the ^{14}N$(\vec{p},\gamma)^{15}$O reaction. The solid curve is the present calculation for an $M1$ resonance and the dashed curve (overlaps solid curve) is for an $E2$ resonance. The dot-dashed curve is the R-matrix calculation of Ref. [4] (scanned). Data were provided by the authors of Ref. [4].

over energy from 252 to 0 keV. Weighting for the integration used both the known stopping powers and calculated cross section as in Eq. (2).

A. Capture to the 6.793-MeV state

The off-resonance direct-capture contribution for capture into the 6.793-MeV ($J^\pi=3/2^+$) state is expected to be dominated by $E1$ radiation from p-wave proton capture. Stripping reactions and shell-model calculations [14] indicate that the $E_{\text{c.m.}}$=259-keV resonance decays to the 6.793-MeV excited state of ^{15}O via $M1$ radiation. The resonance parameters for the 259-keV resonance for the present calculation are taken to be those which best fit the data of Schröder ($J^\pi=1/2^+, \Gamma_\gamma = 1.0\times10^{-2}$ eV, Γ_p=1.0 keV), and are identical to those of Ref. [4] except that the decay mode is taken to be $M1$ rather than $E2$.

For capture to the 6.793-MeV excited state, the interference of an $M1$ or $E2$ resonance at $E_{\text{c.m.}}$=259 keV with the direct $E1$ background reproduces the cross section measured by Schröder and extrapolated in Ref. [4], as shown in Fig. 4. However, an $E2$ resonance interfering with an $E1$ direct-capture amplitude does not give an angular distribution of the analyzing power which resembles the data, as shown in Fig. 5. Even the 135° data point is within 1.5 standard deviations of the calculated analyzing power for an $M1$ resonance, and the $M1$ calculation agreement is much better at 45° and 90°. Either assumption, $M1$ or $E2$ decay, generates an angular distribution for the cross section (Fig. 6) which agrees with the data, highlighting the fact that (unlike analyzing power measurements) these measurements are often insensitive to the detailed nature of the multipoles involved in the reaction. As can be seen in Fig. 4, the difference between the cross section for capture to the 6.793-MeV state calculated in the present case and that calculated in Ref. [4] is under ~20% in the astrophysically interesting energy range, and less than 10% at zero energy. Our conclusion is that the analyzing power data reported here are consistent

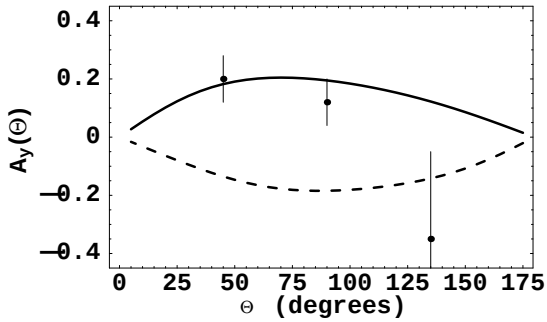

FIG. 5. The analyzing power for capture to the 6.793-MeV state at E_{eff}(c.m.)=245 keV. The solid curve is for an $M1$ resonance with some $E2$ background and the dashed curve is for an $E2$ resonance at $E_{\text{c.m.}}$=259 keV. The error bars are dominated by statistics, although systematic effects have been included.

with the model of an $E1$ direct capture background plus a contribution from the $1/2^+$ resonance at 259 keV. This resonance, however, decays via $M1$ rather than $E2$ radiation as previously assumed [4], consistent with theoretical expectations [14].

B. Capture to the 6.176-MeV state

Capture into the 6.176-MeV ($J^\pi=3/2^-$) state in ^{15}O at low energies should be dominated by $E1$ radiation from s-wave proton capture due to the tail of the $E_{\text{c.m.}}$=259-keV resonance. Capture to the 6.176-MeV state is the strongest mode near the resonance energy and is clearly observed in the present measurement, but has been calculated to drop to less than 10% of the total capture strength at zero energy [4]. The extrapolation of the S factor for capture to this state drops by several orders of magnitude between 252 keV and 0 keV, but the presence of any contribution aside from that of $E1$ resonances has not been considered in these previous extrapolations. We expect the analyzing power to be sensitive to the presence of any non-$E1$ capture strength.

For capture to the 6.176-MeV state, Ref. [4] includes eight $E1$ resonances in order to fit the data of Ref. [2] all

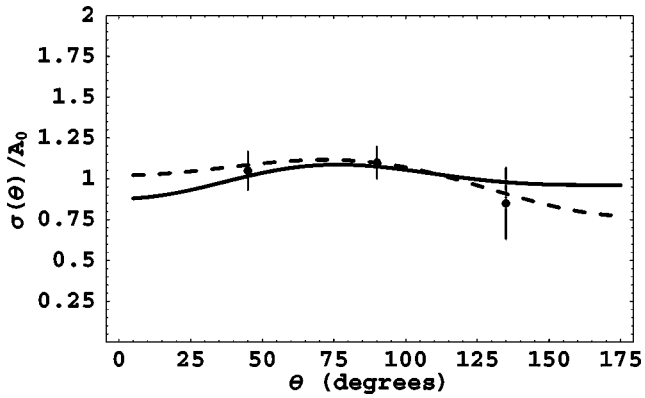

FIG. 6. The angular distribution of the cross section (normalized) for capture to the 6.793-MeV state at E_{eff}(c.m.)=245 keV. The curves indicate similar angular distributions for either an $M1$ (solid curve) or $E2$ (dashed curve) resonance at $E_{\text{c.m.}}$=259 keV.

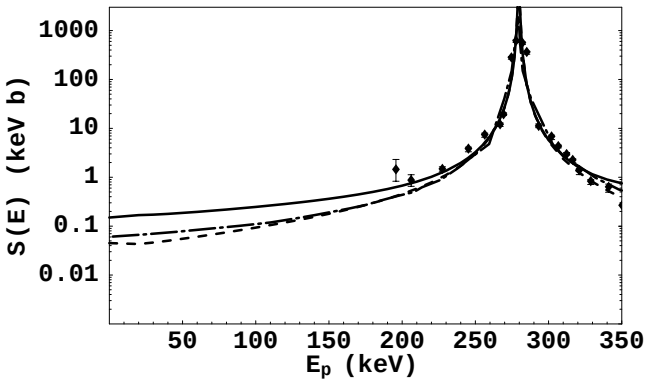

FIG. 7. The S factor for capture to the 6.176-MeV state in ^{15}O in the ^{14}N$(\vec{p}, \gamma)^{15}$O reaction. The present $E1$ only calculation (dashed curve) shown with the previous $E1$ only R-matrix calculation (dot-dashed curve, scanned from Ref. [2]). Data shown are from Ref. [1], provided by the authors of Ref. [2]. The results of a calculation which includes an $M1$ resonance tail is shown as the solid curve.

the way to 2.5 MeV. Our DCPR model using only one $E1$ resonance ($E_{\text{c.m.}}$=259 keV, $J^{\pi}=1/2^{+}$, $\Gamma_{\gamma}=2.0\times10^{-2}$ eV, Γ_{p} =1.0 keV, again identical to the parameters of Ref. [4]) reproduces the previous extrapolation of the S factor [4] up to 350 keV, with the maximum deviation being a 20% undershoot at zero energy (Fig. 7). Above 80 keV the agreement is better than 10%. However, the measured analyzing powers shown in Fig. 8 are large and can be reproduced by the inclusion of an $M1$ background contribution. Direct $M1$ radiation from p-wave protons is already included, but the direct $M1$ strength is negligible. The $M1$ background strength is included in the present model as a resonance with the parameters: $J^{\pi}=3/2^{-}$, Γ_{γ}=1.7 eV, and Γ_{p}=1.5 MeV at $E_{\text{c.m.}}$ =2 MeV. The presence of this small amount of $M1$ strength, 2% of the total capture strength at the effective energy of 248 keV, reproduces the analyzing power much better than $E1$ resonances alone, as shown in Fig. 8. The inclusion of $M1$ strength in the present calculation, required to fit the angular distribution of the analyzing power, does not have a

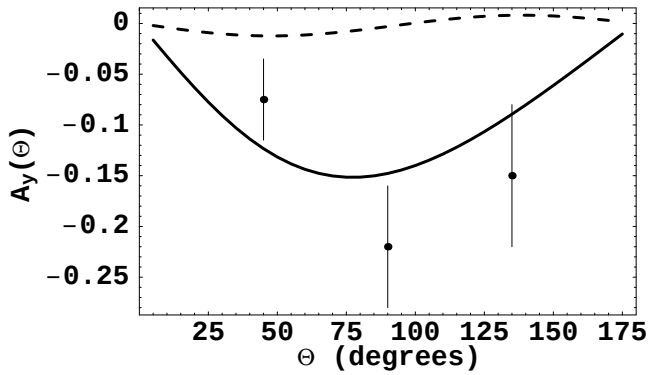

FIG. 8. The analyzing power for capture to the 6.176-MeV state obtained at E_{eff}(c.m.)=248 keV. The dashed curve is for no $M1$ resonance tail and has a shape characteristic of the interference of only $E1$ terms. The solid curve is the result when the tail of an $M1$ background resonance is included, and the shape is again characteristic of $E1$-$M1$ interference.

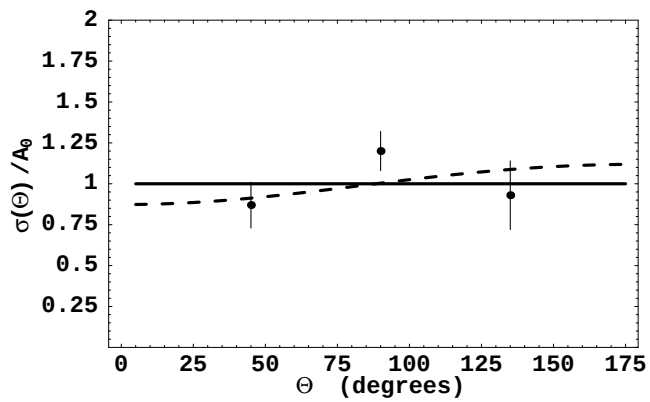

FIG. 9. The normalized angular distribution of the cross section at E_{eff}(c.m.)=248 keV. For the case of $E1$ strength only, we expect (and observe) an isotropic angular distribution (dashed curve). The addition of $M1$ strength (solid curve) results in a 10% asymmetry.

significant effect on the agreement of the calculation with the experimental S-factor data. However, the $M1$ strength contributes significantly to the capture at energies too low to have been measured directly in any experiment to date, increasing the extrapolated $S(0)$ by nearly a factor of 3 to 0.16 keV b. The calculation in the region of the data of Ref. [2] still agrees with that of the R-matrix calculation (within $\approx$10%), as shown in Fig. 7. As with capture to the 6.793-MeV state, it is difficult to tell the difference between the $E1$ and $E1+M1$ angular distributions of the cross section (10% at extreme angles) based on the data (Fig. 9).

IV. CONCLUSIONS

In previous work, cross section data and models were used to extrapolate the S factor of the ^{14}N$(p, \gamma)^{15}$O reaction into the energy region of astrophysical significance. Since analyzing powers are sensitive to the details of the amplitudes involved in the reaction, the present work utilized polarized protons in order to measure the analyzing powers for this reaction. The measured analyzing powers have been used to investigate the simplifying assumption that *only* those multipoles which are ordinarily the most dominant contribute to the S factor at low energies. We have found evidence for the presence of capture amplitudes which were not included in the previous reaction models.

Calculations using the DCPR model generate results consistent with the present polarized proton data. There are few new pieces of information about the details of the capture mechanisms which have been revealed, and which should improve the extrapolations. For capture to the 6.793-MeV state in ^{15}O, our results do not indicate any dramatic change in the extrapolation of the total S factor to low energies. However, our results have verified that the 259-keV resonance decays to the 6.793-MeV state via $M1$ radiation and predict an S factor of 1.50 keV b at zero energy, giving a decrease of 6% in the total S factor for the ^{14}N$(p, \gamma)^{15}$O reaction. In the case of capture to the 6.176-MeV state, we recommend an $S(0)$ of 0.16±0.06 keV b, an increase of a factor of 2.7 compared to previous values. This change arises from the inclusion of $M1$ background strength. The existence

of this $M1$ strength was made clear by the large analyzing powers observed, especially at 90°. It should be noted that this change only increases the total zero-energy S factor for the $^{14}N(p, \gamma)^{15}O$ reaction by about 6%, very nearly canceling the decrease in the S factor which arose from the predictions of the DCPR model for capture to the 6.793-MeV state. The surprising increase in the S factor for capture to the 6.176-MeV state does, however, highlight the need for a detailed investigation of multipoles which typically contribute weakly at high energies, but which may have significant effects at stellar energies.

ACKNOWLEDGMENTS

This work was supported in part by U.S. DOE Grant Nos. DE-FG02-97ER41033, DE-FG02-97ER41042, and DE-FG02-97ER41046.

[1] E. G. Adelberger *et al.*, Rev. Mod. Phys. **70**, 1265 (1998).
[2] U. Schröder *et al.*, Nucl. Phys. **A467**, 240 (1986).
[3] W. A. S. Lamb and R. E. Hester, Phys. Rev. **107**, 550 (1957).
[4] C. Angulo and P. Descouvemont, Nucl. Phys. **A690**, 755 (2001).
[5] R. G. Seyler and H. R. Weller, Phys. Rev. C **20**, 453 (1979).
[6] *Polarization Phenomena in Nuclear Reactions*, edited by H. H. Barschall and W. Haeberli (University of Wisconsin Press, Madison, Wisconsin, 1971).
[7] A. J. Mendez, C. D. Roper, J. D. Dunham, and T. B. Clegg, Rev. Sci. Instrum. **67**, 3073 (1996).
[8] T. B. Clegg, Rev. Sci. Instrum. **61**, 385 (1990).
[9] M. E. Rose, Phys. Rev. **91**, 610 (1953).
[10] A. Artna-Cohen, Nucl. Data Sheets **80**, 723 (1997).
[11] H. H. Andersen and J. F. Ziegler, *The Stopping and Ranges of Ions in Matter* (Pergamon, Elmsford, New York, 1977).
[12] M. C. Wright, H. Kitazawa, N. R. Roberson, and H. R. Weller, Phys. Rev. C **31**, 1125 (1985).
[13] F. Ajzenberg-Selove, Nucl. Phys. **A523**, 1 (1991).
[14] S. Raman *et al.*, Phys. Rev. C **50**, 682 (1994).